Supporting Information

Torsvik et al. 10.1073/pnas.1423099112

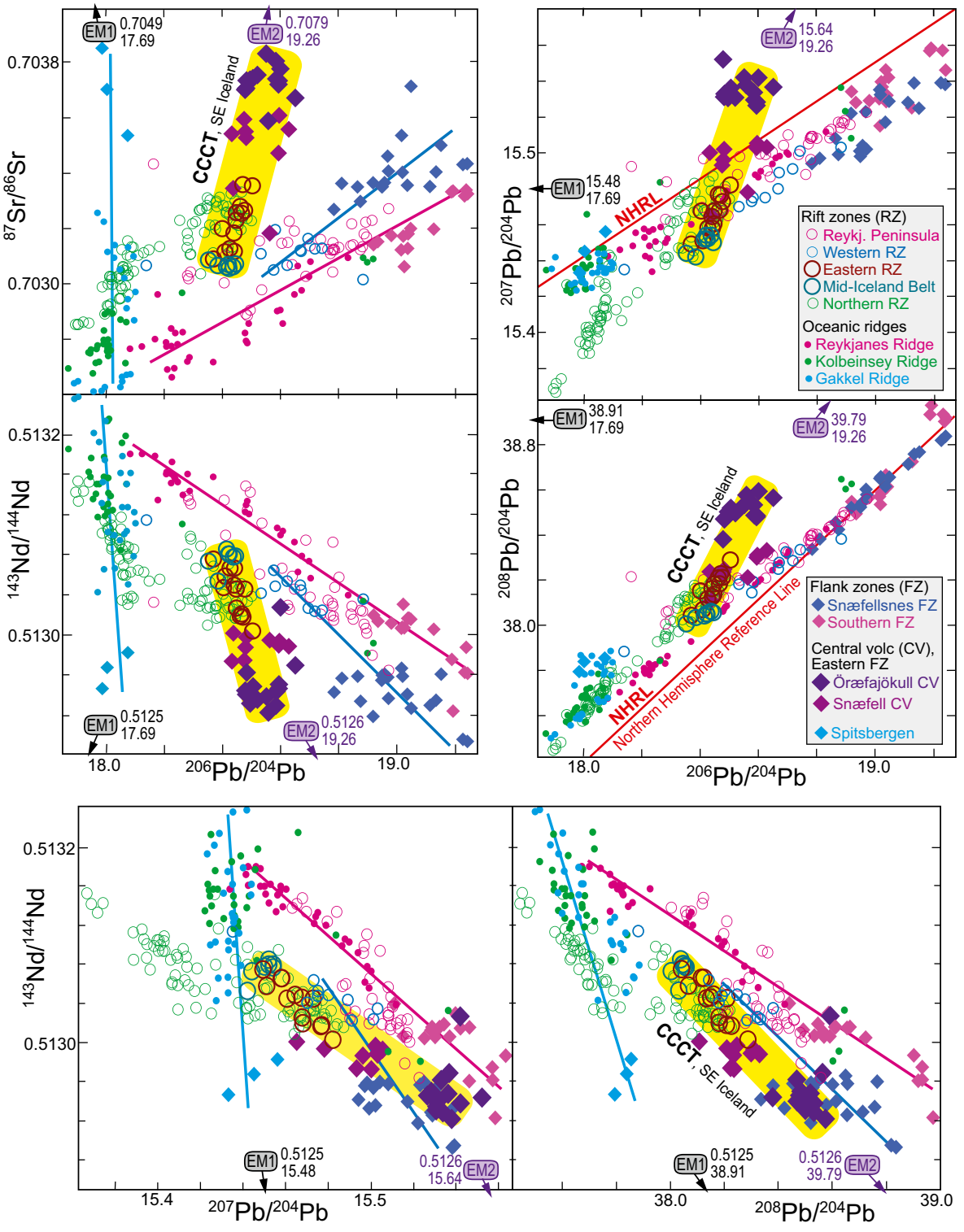

Fig. S1. (Expanded version of Fig. 3.) The Sr–Nd–Pb isotopic composition of basalts from the Icelandic rift and off-rift (flank) zones and the neighboring oceanic spreading ridges. A Continental Crustal Contamination Trend (CCCT) departing from the basalt compositions of the Mid-Icelandic Belt (MIB) via the

Legend continued on following page

Eastern Rift Zone (ERZ) and the Snæfell central volcano at the northern end of the Eastern Flank Zone (EFZ) to Öræfajökull is indicated by yellow shading. Along the well-defined ERZ trend, the distance from the source of individual eruption units to Öræfajökull is generally correlated with the isotope ratios, such that the ERZ samples at the shortest distances are compositionally closest to the EFZ samples. The three guiding lines in the Sr–Pb and Nd–Pb diagrams indicate approximately (not strictly linear regression) the inferred progressive melting trends, involving the following basalt series: (*i*) Spitsbergen via the western to the eastern Gakkel Ridge in the High Arctic; (*ii*) Snæfellsnes to the Western Rift Zone; (*iii*) Southern Flank Zone via the Reykjanes Peninsula to the Reykjanes Ridge. The isotope ratios of the mantle components EM1 and EM2 are given in the each of the diagrams, and the small arrows indicate the approximate directions toward the components. The components are taken as the averages of the most enriched samples with $^{143}Nd/^{144}Nd$ ratios of less than 0.51260 for Pitcairn (EM1) and Samoa (EM2) based on the supplementary table 1 in ref. 1. Data sources are refs. 2–13. Apart from the CCCT from MIB toward the Öræfajökull basalts, the compositional range of basalts from Iceland and the northeast Atlantic and Arctic Oceans can be modeled by mixing and progressive melting of mantle sources, including the Iceland plume with 10% recycled oceanic crust (ROC) and 90% of a diverse lower mantle (containing both melt-depleted and fertile components) and local asthenosphere, contaminated by subcontinental lithospheric mantle (SCLM) (14, 15). The proportion of SCLM increases north of Iceland (the Kolbeinsey, Mohns, and Knipovich Ridges and the Jan Mayen area) and predominates in the Pleistocene to Holocene basalts from Spitsbergen and along the Gakkel Ridge (13–15). The Sr–Pb and Nd–Pb isotope diagrams illustrate various progressive melting trends from fertile to depleted basalts, characterized by variable ROC/SCLM ratios. The highest ROC/SCLM ratio is found in the Southern Flank Zone (SFZ) and the Snæfellsnes Flank Zone, melting to form more depleted basalts of the Reykjanes Peninsula and Ridge and the Western Rift Zone, respectively. The melting trends displayed by basalts from Jan Mayen Island and Jan Mayen Plateau toward the Mohns and Knipovich Ridges (ref. 14; not shown here) represent intermediate ROC/SCLM ratios, whereas the trend from Spitsbergen via the western to the eastern parts of the Gakkel Ridge (High Arctic) have the lowest ROC/SCLM ratios, approaching zero. The Spitsbergen to Gakkel and Southern FZ to Reykjanes melting trends merge at the depleted end of the mid-ocean ridge basalt compositional spectrum, characterized by high Nd- and low Sr- and Pb-isotope ratios. A series of subparallel trends, i.e., from Snæfellsnes FZ via the Western RZ, Northern RZ, and Kolbeinsey Ridge and from Jan Mayen to the Mohns and Knipovich Ridges (not shown), are located between the two extreme Gakkel and Reykjanes melting trends in the various Sr–Pb and Nd–Pb isotope diagrams. The uniqueness of the CCCT is indicated by the fact that it variably intersects the other trends in Sr–Pb and Nd–Pb isotope space. The most prominent feature of the three Nd–Pb diagrams is that the Öræfajökull end of the CCCT points toward low $^{206}Pb/^{204}Pb$, high $^{207}Pb/^{204}Pb$, and intermediate $^{208}Pb/^{204}Pb$ with decreasing $^{143}Nd/^{144}Nd$, e.g., relative to the trend from the Snæfellsnes FZ to the Western RZ. The very low $^{207}Pb/^{204}Pb$ ratios of the picritic lavas from the northern part of the Northern Rift Zone (6) indicate extensive melting of a plume-supplied lower mantle source that was subjected to strong melt depletion early in Earth's history.

1. Stracke A (2012) Earth's heterogeneous mantle: A product of convection-driven interaction between crust and mantle. *Chem Geol* 330-331:274–299.
2. Prestvik T, Goldberg S, Karlsson H, Grönvold K (2001) Anomalous strontium and lead isotope signatures in the off-rift Öræfajökull central volcano in south-east Iceland. Evidence for enriched endmember(s) of the Iceland mantle plume? *Earth Planet Sci Lett* 190:211–220.
3. Kokfelt TF, et al. (2006) Combined trace element and Pb-Nd-Sr-O isotope evidence for recycled oceanic crust (upper and lower) in the Iceland mantle plume. *J Petrol* 47(9):1705.
4. Peate DW, et al. (2010) Compositional characteristics and spatial distribution of enriched Icelandic mantle components. *J Petrol* 51(7):1447–1475.
5. Schilling J-G, Kingsley R, Fontignie D, Poreda R, Xue S (1999) Dispersion of the Jan Mayen and Iceland mantle plumes in the Arctic: A He-Pb-Nd-Sr isotope tracer study of basalts from the Kolbeinsey, Mohns, and Knipovich Ridges. *J Geophys Res* 104:10543–10569.
6. Stracke A, et al. (2003) Theistareykir revisited. *Geochem Geophys Geosyst* 4:2001GC000201.
7. Thirlwall MF, Gee MAM, Taylor RN, Murton BJ (2004) Mantle components in Iceland and adjacent ridges investigated using double-spike Pb isotope ratios. *Geochim Cosmochim Acta* 68(2):361–386.
8. Manning CJ, Thirlwall MF (2014) Isotopic evidence for interaction between Öræfajökull mantle and the Eastern Rift Zone, Iceland. *Contrib Mineral Petrol* 167(1):10.1007/s00410-013-0959-1–22.
9. Blichert-Toft J, et al. (2005) Geochemical segmentation of the mid-Atlantic ridge north of Iceland and ridge-hot spot interaction in the north Atlantic. *Geochem Geophys Geosyst* 6(1): Q01E19.
10. Peate DW, et al. (2009) Historic magmatism on the Reykjanes Peninsula, Iceland: A snap-shot of melt generation at a ridge segment. *Contrib Mineral Petrol* 157:359–382.
11. Shorttle O, Maclennan J, Piotrowski AM (2013) Geochemical provincialism in the Iceland plume. *Geochim Cosmochim Acta* 122:363–397.
12. Ionov DA, Mukasa SB, Bodinier J-L (2002) Sr-Nd-Pb isotopic compositions of peridotite xenoliths from Spitsbergen: Numerical modelling indicates Sr-Nd decoupling in the mantle by melt percolation metasomatism. *J Petrol* 43(12):2261–2278.
13. Goldstein SL, et al. (2008) Origin of a "Southern Hemisphere" geochemical signature in the Arctic upper mantle. *Nature* 453(7191):89–93.
14. Trønnes RG, Debaille V, Erambert M, Stuart FM, Waight T (2013) Mixing and progressive melting of deep and shallow mantle sources in the NE Atlantic and Arctic (abstract, Goldschmidt Conf.). *Mineral Mag* 77:2357.
15. Debaille V, et al. (2009) Primitive off-rift basalts from Iceland and Jan Mayen: Os-isotopic evidence for a mantle source containing enriched subcontinental lithosphere. *Geochim Cosmochim Acta* 73(11):3423–3449.

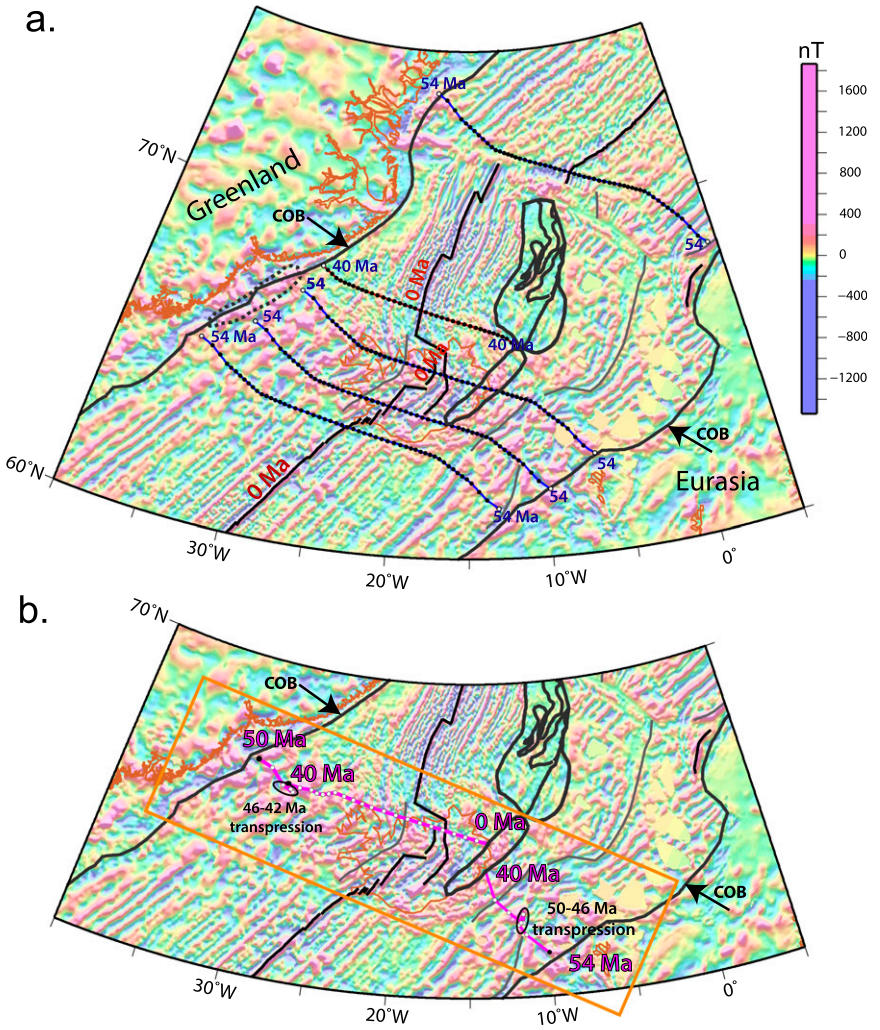

Fig. S2. (*A*) Flow lines showing the direction and amount of (symmetric) seafloor spreading between Eurasia and Greenland and between Greenland and JMM calculated in 2-My time intervals from stage poles derived from the Gaina et al. (1) kinematic model. That model was derived from magnetic anomalies identified north and south of Iceland. The base map shows the total magnetic anomaly grid of the northeast Atlantic (2). Thin dark gray lines represent the identified continent–ocean boundaries (COBs). Note the position and extent of JMM-E (dashed line) next to the Greenland COB in a reconstructed (54 Ma) position. (*B*) Motion path of JMM-E relative to Eurasia (magenta lines east of JMM-E) and of the JMM-E relative to Greenland (magenta lines west of JMM-E) in 2-My intervals. Due to competing midocean-ridge propagation from northeast (the Ægir Ridge) and from southwest (the Reykjanes ridge) between 50 and 42 Ma, JMM-E experienced rotation, and its boundaries with surrounding continental and oceanic crust were subjected to transpression and strike–slip motion (see motion path segments within the black ellipses). This time interval coincided with major reorganizations in the northeast Atlantic suggested by changes in seafloor spreading directions and rates (1, 3). Due to these tectonic events and magmatic overprint from the Iceland plume, the magnetic anomaly data show a quasichaotic pattern across the Iceland-Faroe ridge (orange rectangle).

1. Gaina C, Gernigon L, Ball P (2009) Palaeocene—Recent plate boundaries in the NE Atlantic and the formation of the Jan Mayen microcontinent. *J Geol Soc London* 166:601–616.
2. Gaina C, Werner S, Saltus R, Maus S, CAMP-GM Group (2011) Circum-Arctic Mapping Project: New magnetic and gravity anomaly maps of the Arctic. *Arctic Petroleum Geology*, eds Spencer AM, Embry AF, Gautier DL, Stoupakova AV, Sørensen K, Geological Society London, Memoirs (Geological Society, London), Vol 35, pp 39–48.
3. Gernigon L, et al. (2012) The Norway Basin revisited: From continental breakup to spreading ridge extinction. *Mar Pet Geol* 35:1–19.

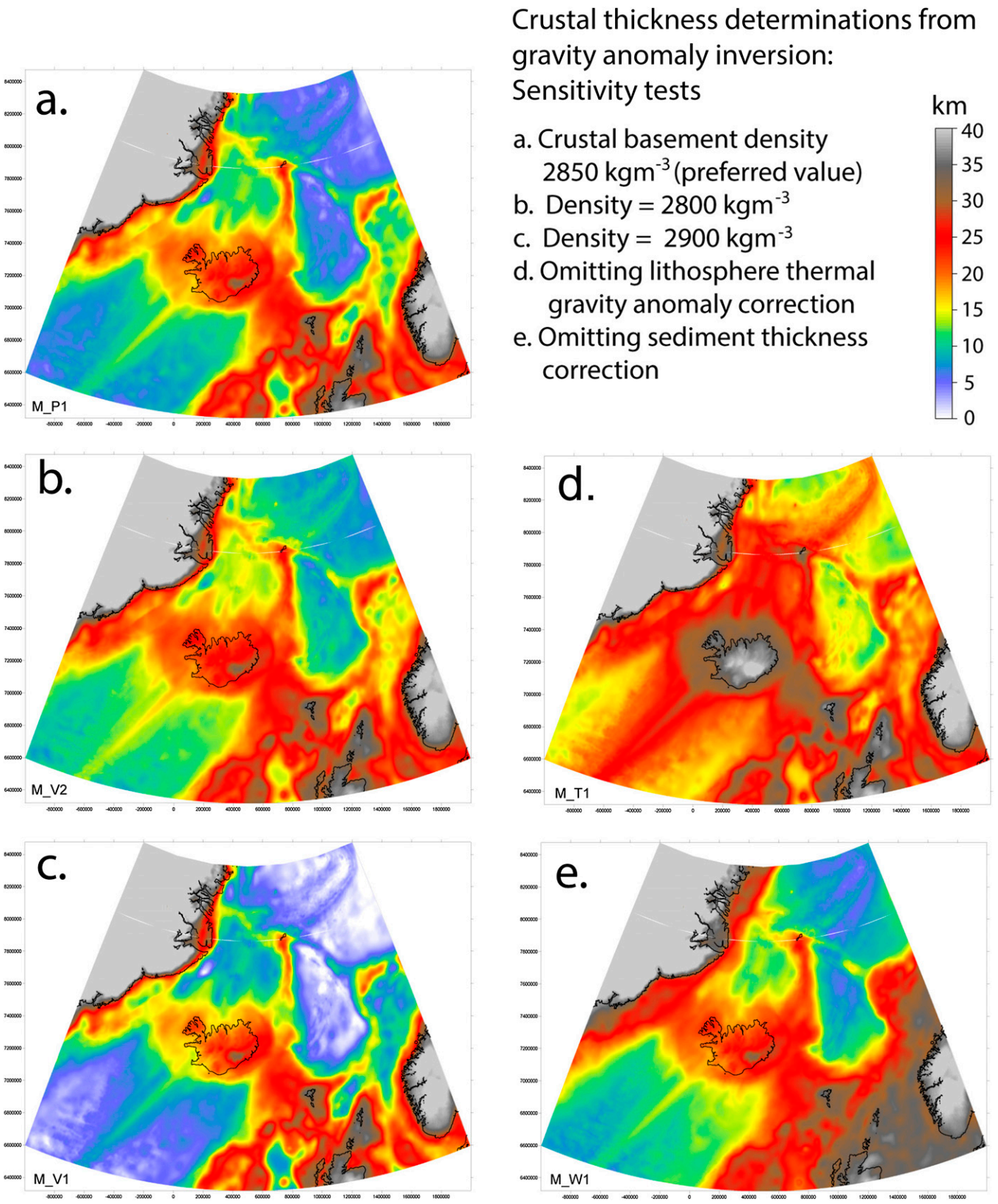

Fig. S3. Crustal thickness maps derived from gravity anomaly inversion (detailed in refs. 1–3) showing sensitivity to crustal basement density, lithosphere thermal gravity anomaly correction, and sediment thickness correction. (*A*) Crustal basement density, 2,850 kg·m^{-3} (preferred value, as in Fig. 1). (*B*) Crustal basement density, 2,800 kg·m^{-3}. (*C*) Crustal basement density, 2,900 kg·m^{-3}. (*D*) Omitting a lithosphere thermal gravity anomaly correction results in the prediction of a Moho that is too deep and a crustal thickness that is too large (1). The lithosphere thermal gravity anomaly correction is calculated using a 3D lithosphere thermal model incorporating the spatial variation in the initial lithosphere thermal perturbation and thermal reequilibration (i.e., cooling) time.

Legend continued on following page

The lithosphere thermal perturbation for breakup and seafloor spreading is defined using the lithosphere thinning factors ($1 - 1/\beta$) and the model of McKenzie (4). For continental lithosphere, this thinning factor is derived from the gravity inversion; for oceanic lithosphere, it may also be derived from the gravity inversion or alternatively may be set to 1 (corresponding to β = infinity), where a priori reliable ocean isochron data exist (Fig. 8*B*). For continental margin lithosphere, the cooling time is breakup age; for oceanic lithosphere, the cooling time is the ocean isochron age. Errors in ocean isochron location and age cause errors in the lithosphere thermal gravity anomaly correction and as a consequence the Moho depth, crustal thickness, and lithosphere thinning derived from gravity inversion. Therefore, the oldest isochrons adjacent to the continent–ocean boundary are not usually used in the gravity inversion; in this study, a continental breakup age of 55 Ma is assumed for the northeast Atlantic and the oldest ocean isochron used is 50 Ma (about chron 22 time in Fig. 8*A*). Sensitivity tests have also been carried out to the use of isochrons to condition the 3D lithosphere thermal model used to calculate the lithosphere thermal gravity anomaly correction incorporated in the gravity inversion. These tests show that the predicted thicker crust under JMM and southeast Iceland are not significantly dependent on ocean-age isochrons used to determine the lithosphere thermal gravity anomaly correction, and that the thicker crust under the JMM, compared with that of the oceanic basins to the east and west, extends southwestward into southeast Iceland. (*E*) Omitting the sediment thickness gravity anomaly contribution from the gravity inversion (or using too small sediment thickness) leads to an overestimate of Moho depth and crustal basement thickness. The sediment thickness grid used in this study is a merge of the Divins (5) and Laske et al. (6) compilations, and sediment density used in the gravity inversion assumes a compaction-controlled density–depth relationship. The same reference Moho depth of 35 km is used for gravity inversion solutions *A*, *B*, and *C*.

1. Chappell AR, Kusznir NJ (2008) Three-dimensional gravity inversion for Moho depth at rifted continental margins incorporating a lithosphere thermal gravity anomaly correction. *Geophys J Int* 174:1–13.
2. Greenhalgh EE, Kusznir NJ (2007) Evidence for thin oceanic crust on the extinct Aegir Ridge, Norwegian Basin, NE Atlantic derived from satellite gravity inversion. *Geophys Res Lett* 34(6):L06305.
3. Alvey A, Gaina C, Kusznir NJ, Torsvik TH (2008) Integrated crustal thickness mapping and plate reconstructions for the High Arctic. *Earth Planet Sci Lett* 274:310–321.
4. McKenzie D (1978) Some remarks on the development of sedimentary basins. *Earth Planet Sci Lett* 40:25.
5. Divins DL (2008) Total sediment thickness of the World's oceans and marginal seas. NGDC. Available at https://www.ngdc.noaa.gov/mgg/sedthick/sedthick.htm. Accessed May 21, 2014.
6. Laske G, Masters G (1997) A global digital map of sediment thickness. *Eos Trans AGU* 78:F483.

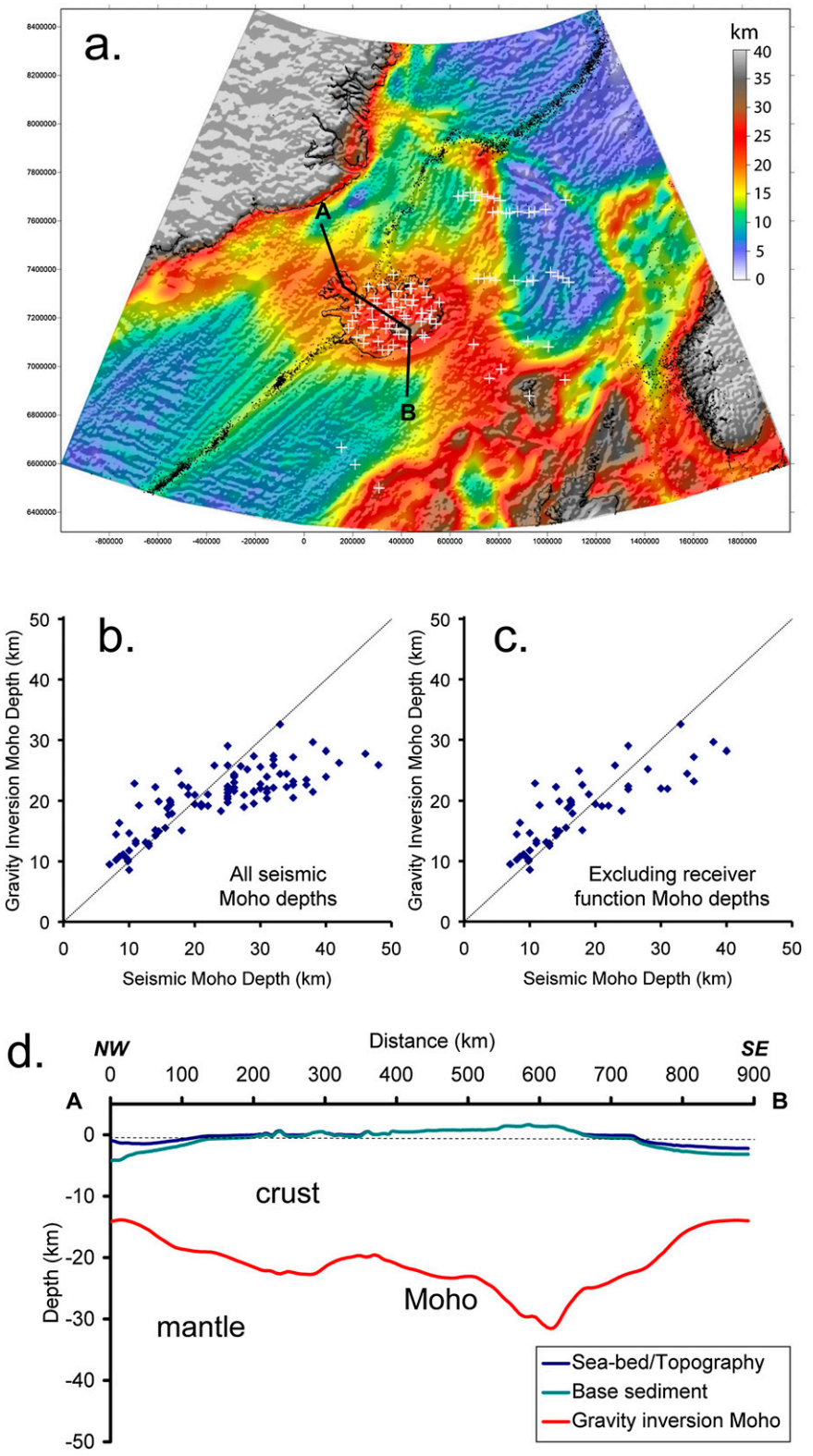

Fig. S4. (*A*) Location of seismically determined Moho depth measurements (white +) for comparison with Moho depths determined from gravity inversion (as in Fig. 1). (*B*) Cross-plot of gravity versus seismically (1–16) determined Moho depths. (*C*) Cross-plot excluding seismically determined Moho depth using receiver function analysis. Cross-plots show a good correlation, but at larger Moho depths, seismic values are consistently greater than gravity-determined values, suggesting that the gravity inversion may be underestimating Moho depths. One explanation for this may be that that the densities of thicker (or deeper) crust may be larger than the preferred value of 2,850 kg·m^{-3} used in the gravity inversion. Some of the seismic Moho depth determinations are large, exceeding 40 km; some of these large values correspond to receiver function determinations that may be overestimating Moho depth. (*D*) Crustal cross-section A–B with

Legend continued on following page

Moho depth determined using gravity inversion. The crustal cross-section—running from the northern Denmark Strait across Iceland from Snæfellnes to Öræfajökull and then into the northeast Iceland Basin—shows thickest crust under southeast Iceland.

1. Darbyshire FA, White RS, Priestley KF (2000) Structure of the crust and uppermost mantle of Iceland from a combined seismic and gravity study. *Earth Planet Sci Lett* 181:409–428.
2. Darbyshire FA, et al. (2000) Crustal structure of central and northern Iceland from analysis of teleseismic receiver functions. *Geophys J Int* 143:163–184.
3. Kumar P, Kind R, Priestley K, Dahl-Jensen T (2007) Crustal structure of Iceland and Greenland from receiver function studies. *J Geophys Res* 112(B3):B03301.
4. Foulger GR (2006) Older crust underlies Iceland. *Geophys J Int* 165:672–676.
5. Breivik AJ, Mjelde R, Faleide JI, Murai YJ (2006) Rates of continental breakup magmatism and seafloor spreading in the Norway Basin-Iceland plume interaction. *J Geophys Res* 111(B7): B07102.
6. Breivik AJ, Mjelde R, Faleide JI (2008) Neogene magmatism northeast of the Aegir and Kolbeinsey ridges, NE Atlantic: Spreading ridge mantle plume interaction? *Geochem Geophys Geosyst* 9(2):Q02004.
7. Breivik AJ, Mjelde R, Faleide JI, Muro Y (2012) The eastern Jan Mayen microcontinent volcanic margin. *Geophys J Int* 188:798–818.
8. Bohnhoff M, Makris J (2004) Crustal structure of the southeastern Iceland-Faeroe Ridge (IFR) from wide aperture seismic data. *J Geodyn* 37:233–252.
9. Harland KE, White RS, Soosalu H (2009) Crustal structure beneath the Faroe Islands from teleseismic receiver functions. *Geophys J Int* 177:115–124.
10. Kodeira S, Mjelde R, Gunnarsson K, Shiobara H, Shimamura H (1998) Structure of the Jan Mayen microcontinent and implication for its evolution. *Geophys J Int* 132:383–400.
11. Kodeira S, Mjelde R, Shiobara H, Shimamura H (2002) Evolution of oceanic crust on the Kolbeinsey Ridge, north of Iceland, over the past 22 Myr. *Terra Nova* 10(1):27–31.
12. Mjelde R, et al. (2008) Magmatic and tectonic evolution of the North Atlantic. *J Geol Soc Lond* 165:31–42.
13. Mjelde R, Aurvåg R, Kodaira S, Shimamura H, Gunnarsson K (2002) Vp/Vs-ratios from the central Kolbeinsey ridge to the Jan Mayen basin, North Atlantic; implications for lithology, porosity and present-day stress field. *Mar Geophys Res* 23:125–145.
14. Richardson KR, Smallwood JR, White RS, Snyder DB, Maguire PKH (1998) Crustal structure beneath the Faroe Islands and the Faroe–Iceland Ridge. *Tectonophysics* 300:159–180.
15. White RS, et al. (2008) Lower-crustal intrusion on the North Atlantic continental margin. *Nature* 452(7186):460–464.
16. White RS, Smith LK (2009) Crustal structure of the Hatton and the conjugate east Greenland rifted volcanic continental margins, NE Atlantic. *J Geophys Res* 114(B2):B02305.

Table S1. Absolute reconstruction parameters (Euler poles) for the Cenozoic

Age, Ma	Continent, microcontinent	Latitude, °	Longitude, °	Angle, °
27	Greenland (as North America)	51.3	131.8	5.5
	All Jan Mayen Blocks and Eurasia	58.7	316.6	−2
33	Greenland	53.8	125	6.6
	Jan Mayen/Jan Mayen South*	65.5	337.7	−12.3
	Jan Mayen Extended	52.8	40.8	2.4
	Eurasia	59.1	293.6	−2.1
40	Greenland	44.5	114.9	7.5
	Jan Mayen	55.3	310.4	−8
	Jan Mayen South*	65.6	326	−16.6
	Jan Mayen Extended	18	253.9	−2.6
	Eurasia	50.3	264.6	−2.7
45	Greenland	47.2	107.8	7.8
	Jan Mayen	58.3	309.3	−9.6
	Jan Mayen South*	66.3	324.3	−18.2
	Jan Mayen Extended	47.8	31	6.5
	Eurasia	42.4	224.5	−2.5
52	Greenland	45.6	98.1	9.2
	Jan Mayen	61.2	313.7	−15.7
	Jan Mayen South*	65.9	324.3	−24.3
	Jan Mayen Extended	53.5	264.5	−6.1
	Eurasia	27.7	200.6	−3.4
55†	Greenland	46.9	101.6	8.8
	Jan Mayen	62.9	321.5	−18.3
	Jan Mayen South*	66.4	329.5	−27
	Jan Mayen Extended	21	240	−3.6
	Eurasia	30.9	208.2	−2.9
60†	Greenland	47.1	89.7	9.3
	Jan Mayen	62.7	308.4	−16
	Jan Mayen South*	67.5	320.3	−24.7
	Jan Mayen Extended	65.1	286.3	−11.1
	Eurasia	29.6	178.7	−5.2

*The Jan Mayen Microcontinent block marked S in Fig. 8*B*.
†Reconstructions at 55 and 60 Ma include minor prebreakup extension. Estimated prebreakup extension for Eurasia relative Greenland based on Gaina et al. (1).

1. Gaina C, Roest WR, Muller RD (2002) Late Cretaceous-Cenozoic deformation of northeast Asia. *Earth Planet Sci Lett* 197:273–286.

Table S2. Euler poles for relative motion versus a fixed Greenland

Age, Ma	Continent, microcontinent	Latitude, °	Longitude, °	Angle, °
27	All Jan Mayen Blocks and Eurasia	68.5	131.9	−6.5
33	Jan Mayen/Jan Mayen South*	82.3	20.8	−16.7
	Jan Mayen Extended	39.3	145.3	−5.2
	Eurasia	68.2	131.5	−7.6
40	Jan Mayen	84.6	75.8	−11.9
	Jan Mayen South*	82.6	9.2	−20.7
	Jan Mayen Extended	56.6	141.6	−7.2
	Eurasia	60.0	129.5	−8.3
45	Jan Mayen	84.5	40.4	−14.1
	Jan Mayen South*	81.5	3.6	−22.9
	Jan Mayen Extended	6.9	149.7	−6.2
	Eurasia	56.3	128.9	−8.9
52	Jan Mayen	80.9	8.3	−20.7
	Jan Mayen South*	79.1	358.4	−29.6
	Jan Mayen Extended	74.2	122.4	−11.9
	Eurasia	50.0	125.1	−10.4
55†	Jan Mayen	80.7	4.1	−21.5
	Jan Mayen South*	79	356.9	−30.4
	Jan Mayen Extended	83.9	73.2	−17
	Eurasia	52.4	123.5	−12.0
60†	Jan Mayen	80.7	4.1	−21.52
	Jan Mayen South*	79.2	357.6	−30.4
	Jan Mayen Extended	83.9	73.2	−17
	Eurasia	48.3	124.5	−12.2

*The Jan Mayen Microcontinent block marked S in Fig. 8*B*.
†Reconstructions at 55 and 60 Ma include minor prebreakup extension. Estimated prebreakup extension for Eurasia relative Greenland based on Gaina et al. (1).

1. Gaina C, Roest WR, Muller RD (2002) Late Cretaceous-Cenozoic deformation of northeast Asia. *Earth Planet Sci Lett* 197:273–286.

Other Supporting Information Files

Dataset S1 (XLSX)